

Article

Real-Time Estimation of Low Earth Orbit (LEO) Satellite Clock Based on Ground Tracking Stations

Zhixin Yang ¹, Hui Liu ¹, Chuang Qian ¹, Bao Shu ², Linjie Zhang ¹, Xintong Xu ¹, Yi Zhang ³ and Yidong Lou ^{1,*}

¹ GNSS Research Center, Wuhan University, Wuhan 430079, China; zhixinyang@whu.edu.cn (Z.Y.); liuhui@wnlbs.com (H.L.); qc_gnss@whu.edu.cn (C.Q.); zhang71@whu.edu.cn (L.Z.); xuxintonggnss@whu.edu.cn (X.X.)

² College of Geological Engineering and Geomatics, Chang'an University, Xi'an 710054, China; baos613@163.com

³ Zhejiang GeeSpace Technology Co., Ltd., Shanghai 200233, China; 15801520938@126.com

* Correspondence: ydlou@whu.edu.cn

Received: 18 May 2020; Accepted: 23 June 2020; Published: 25 June 2020



Abstract: The rapid movement of low Earth orbit (LEO) satellite can improve geometric diversity, which contributes to the rapid convergence of Global Navigation Satellite System (GNSS) precise point positioning (PPP). However, the LEO onboard receiver clock cannot be used directly by PPP users as the LEO satellite clock because the LEO onboard receiver clock and LEO satellite clock absorb different code delays when receiving and transmitting signals. In this study, a real-time estimation approach for the LEO satellite clock based on ground tracking stations was proposed for the first time. The feasibility for the rapid convergence of the LEO satellite clock was analyzed using the satellite time dilution of precision (TDOP) that one satellite is relative to multiple ground tracking stations. The LEO constellation of 168 satellites and observations for 15 ground tracking stations were simulated to verify the proposed method. The experiment results showed that the average convergence time was 31.21 min for the Global Positioning System (GPS) satellite clock, whereas the value for the LEO satellite clock was only 2.86 min. The average root mean square (RMS) and standard deviation (STD) values after convergence were 0.71 and 0.39 ns for the LEO satellite clock, whereas the values were 0.31 and 0.13 ns for the GPS satellite clock. The average weekly satellite TDOP for the LEO satellite was much smaller than that for the GPS satellite. The average satellite TDOPs for all LEO and GPS satellites were 19.13 and 1294.70, respectively. However, the average delta TDOPs caused by satellite motion for all LEO and GPS satellites were both 0.10. Therefore, the rapid convergence of the LEO satellite clock resulted from the better geometric distribution of the LEO satellite relative to ground stations. Despite errors and the convergence time of the LEO satellite clock, the convergence time and positioning accuracy for LEO-augmented GPS and BeiDou Navigation Satellite System (BDS) PPP with the real-time estimated LEO satellite clock can still reach 10.63 min, 1.94 cm, 1.44 cm, and 4.18 cm in the east, north, and up components, respectively. The improvements caused by LEO satellite for GPS/BDS PPP were 59%, 30%, 31%, and 33%, respectively.

Keywords: LEO constellation; satellite clock estimation; ground tracking stations; precise point positioning (PPP)

1. Introduction

As an absolute positioning technology suitable for large areas with high precision, precise point positioning (PPP) has developed into one of the most representative technologies in Global Navigation Satellite System (GNSS) precise positioning [1]. Nowadays, PPP has been widely used in many

areas with positioning, navigation, and timing (PNT) services due to its advantages of cost efficiency and accuracy satisfactory [1–4]. Multi-GNSS has great potential to improve the performance of PPP considerably, and the convergence time and positioning accuracy can be improved by approximately 70% and 25% compared with that of Global Positioning System (GPS) [2,3,5]. The root mean square (RMS) values of real-time GNSS PPP positioning errors can reach 1.5, 1.7, and 4.7 cm in the north, east, and up components, respectively [6]. However, real-time PPP still has the problems of long convergence time and the precise orbit and clock products' latency. The geometry change of the GNSS satellite relative to the ground station is excessively slow, such that approximately 20 minutes are required to complete the PPP convergence process due to the high orbit altitude [4,7]. These problems of GNSS PPP limit its adoption in time-critical applications, especially in real-time applications [8]. Therefore, how to improve the convergence time of multi-GNSS PPP dramatically remains an urgent problem to be solved.

Since the International Telecommunication Union reported six filings for the spectrum allocation of large low Earth orbit (LEO) constellation in late 2014 and early 2015, the LEO constellation has received more attention in the satellite industry [9–11]. Several commercial companies, for instance, OneWeb, SpaceX, Samsung, Boeing, and Telesat, declared their plan about LEO constellation with hundreds to thousands of satellites to provide global and robust broadband coverage [12–16]. These large LEO constellations provide opportunities for broadband and PNT services by broadcasting navigation signals [17]. LEO satellites have a lower orbital altitude, between 400 and 1500 km, and the faster motion than GNSS satellites. These characteristics of LEO satellites contribute to the rapid changes of geometric distribution and the rapid convergence of PPP. Therefore, the LEO constellation is expected to enhance geometric diversity and enhance the performance of GNSS PPP effectively.

Considerable research has been conducted on the basis of theories and simulations to realize advantageous complementarities on LEO constellations. For example, Reid et al. [17] explored the full architecture of leveraging commercial constellations for navigation, from user geometry and ranging errors to position errors. The results indicated that the commercial LEO constellations for navigation have the potential to add remarkable benefits to protect, toughen, and augment PNT services. Ke et al. [18] adopted a combined PPP model GPS and LEO satellites to verify the improvement of LEO to GPS and found that this combined model can shorten PPP convergence time. Li et al. [19] researched the performance of LEO-augmented multi-GNSS for rapid PPP convergence with six simulated LEO constellations. The results indicated that the LEO constellation with 192 satellites and the orbit altitude of 1000 km had better performance, and the convergence time of GNSS PPP can be shortened to a few minutes with the augmentation of LEO satellites. The geometric dilution of precision (GDOP) and the number of visible satellites of LEO constellation were evaluated by Ge et al. [20], and the experimental results showed that LEO constellation-enhanced GNSS can shorten PPP convergence to 5 min. Li et al. [21] estimated the uncalibrated phase delay of GNSS and LEO using simulated data, and the results showed that the characteristic of LEO uncalibrated phase delay (UPD) is similar to that of GPS UPD. Li et al. [22] investigated the feasibility of LEO-enhanced GNSS (LeGNSS) for providing real-time PPP services, including precise orbit and clock products of GNSS and LEO satellites. The results indicated that improved schemes can balance the computation burden and the accuracy of orbit detection, and achieve enhanced orbit and clock precision similar to the one-step method.

Nevertheless, most researchers have ignored the issue of the LEO satellite clock estimation and utilized the simulated precise clock of the LEO satellite in the processing strategy of LEO-augmented GNSS PPP [19–21,23]. For instance, Li et al. [22] imposed equal constraints on the LEO onboard receiver clock and the LEO satellite clock when estimating clocks. However, the LEO onboard receiver clock and LEO satellite clock are unequal because they absorb different code delays when receiving and transmitting signals. That is, the LEO onboard receiver clock cannot be used directly by PPP users as the LEO satellite clock. Since the LEO satellite serves as the navigation satellite to transmit navigation signals, the determination of the LEO satellite clock must rely on ground tracking stations. The characteristic of the difference between the two clocks remains unclear, which makes this difference

impossible to estimate by combining the observations from ground and LEO onboard receivers. Therefore, a real-time estimation approach for the LEO satellite clock based on ground tracking stations with simulated observations was proposed in this study. The convergence time in the estimation process and the accuracy after convergence for the LEO satellite clock were analyzed compared with those for GPS satellites. The feasibility for the rapid convergence of the LEO satellite clock was evaluated using the satellite time dilution of precision (TDOP) that one satellite is relative to multiple ground tracking stations. The performance of LEO-augmented GNSS PPP solutions with the real-time estimated LEO satellite clock was analyzed. Only if the LEO satellite clock is estimated accurately can the LEO constellation play a role in augmenting GNSS PPP.

After this introduction, this study is structured as follows. Constellations for LEO, GPS, and BeiDou Navigation Satellite System (BDS) and observations for 15 ground tracking stations are simulated in Section 2. In Section 3, the approach for the LEO satellite clock estimation and the LEO-augmented GNSS PPP with the estimated LEO satellite clock are introduced. In Section 4, the convergence speed, accuracy of satellite clock, and satellite TDOP are analyzed to assess the quality of the estimated LEO satellite clock, and the performance of LEO-augmented GNSS PPP with the real-time estimated clock is assessed. Then, the discussion is given in Section 5. Lastly, the conclusions from our results are provided in Section 6.

2. Constellation and Observation Simulation

There are no available LEO satellite observations from ground stations for experimental analysis and verification. In this section, constellations for LEO, GPS, and BDS-3 and observations for 15 ground tracking stations from the day of year (DOY) 305 to 311, 2019 were simulated to verify the estimation approach for the LEO satellite clock and the performance of LEO-augmented GNSS PPP with the estimated LEO satellite clock.

2.1. Constellation Design

The LEO, GPS, and BDS-3 constellations were simulated with Systems Tool Kit (STK) software. The LEO constellation designed by Zhejiang GeeSpace Technology Co., Ltd., was used in this study. This constellation has 168 LEO satellites and consists of two sub-constellations, A and B [24]. The LEO sub-constellation A consists of 132 satellites, operates in the orbit altitude of 800 km with 50° inclination angle, and uses a Walker 132/12/1 constellation geometry. The LEO sub-constellation B consists of 36 satellites, operates in the orbit altitude of 820 km with 85° inclination angle, and uses a Walker 36/3/0 constellation geometry. The Walker constellation was introduced by Walker J.G. [25] and can be described as three parameters. GPS and BDS-3 constellations were also simulated to compare and analyze the clock with LEO satellites based on their nominal parameter configurations [26,27]. The GPS constellation consists of 24 medium earth orbit (MEO) satellites, and operates in six orbital planes with 55° inclination angle at 20,200 km in altitude. The BDS-3 constellation consists of three geostationary earth orbit (GEO) satellites, three inclined geosynchronous orbit (IGSO) satellites, and 24 MEO satellites. The BDS GEO satellites operate in the orbit altitude of 35,786 km, located at 80° E, 110.5° E, and 140° E. BDS IGSO satellites have the same altitude as GEO with 55° inclination angle, and the right ascension of the ascending node (RAAN) is 118° E. The BDS MEO satellites employ a Walker 24/3/1 constellation geometry, which operates in an orbit altitude of 21,528 km and inclination of 55°. Table 1 shows the constellation parameters of LEO, GPS, and BDS-3.

Figure 1 shows the simulation for the designed LEO constellation, which consists of A and B, two sub-constellations. Figure 2 depicts the global distribution for the average number of the visible satellite and the position dilution of precision (PDOP) of the designed LEO constellation. The global distribution of the average number of visible LEO satellites and PDOP values shown in Figure 2 is consistent. It can be seen that the number of visible LEO satellites and the PDOP value are better in the middle latitudes' region than in the low latitudes' region, and better in the low latitudes' region than in the high latitudes' region. Therefore, the combination constellation designed in this study

allowed more LEO satellites to be observed in the regions of middle latitudes and several satellites to be observed in polar regions.

Table 1. low Earth orbit (LEO), Global Positioning System (GPS), and BeiDou Navigation Satellite System (BDS) constellation information.

System	Satellite Number	Constellation	Inclination [deg]	Altitude [km]
LEO A	132	Walker (132/12/1)	50	800
LEO B	36	Walker (36/3/0)	85	820
GPS	24	Six planes	56	20,180
BDS MEO	24	Walker (24/3/1)	55	21,528
BDS GEO	3	Placed at 80° E, 110.5° E, 140° E	0	35,786
BDS IGSO	3	RAAN of 118° E	55	35,786

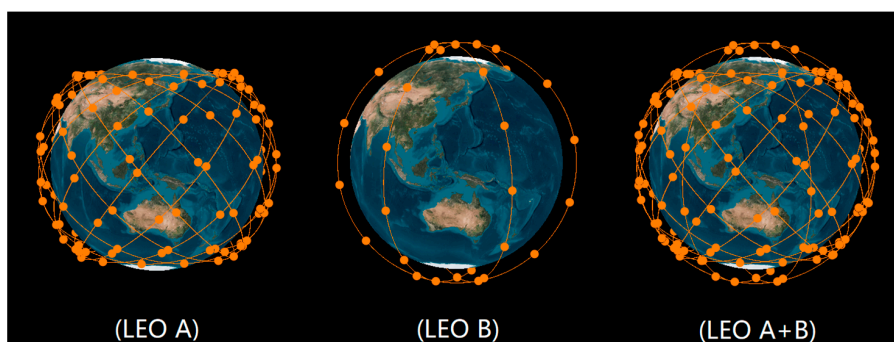


Figure 1. Designed low Earth orbit (LEO) constellation simulation. LEO A and B are two LEO sub-constellations, and LEO A+B is an integrated LEO constellation.

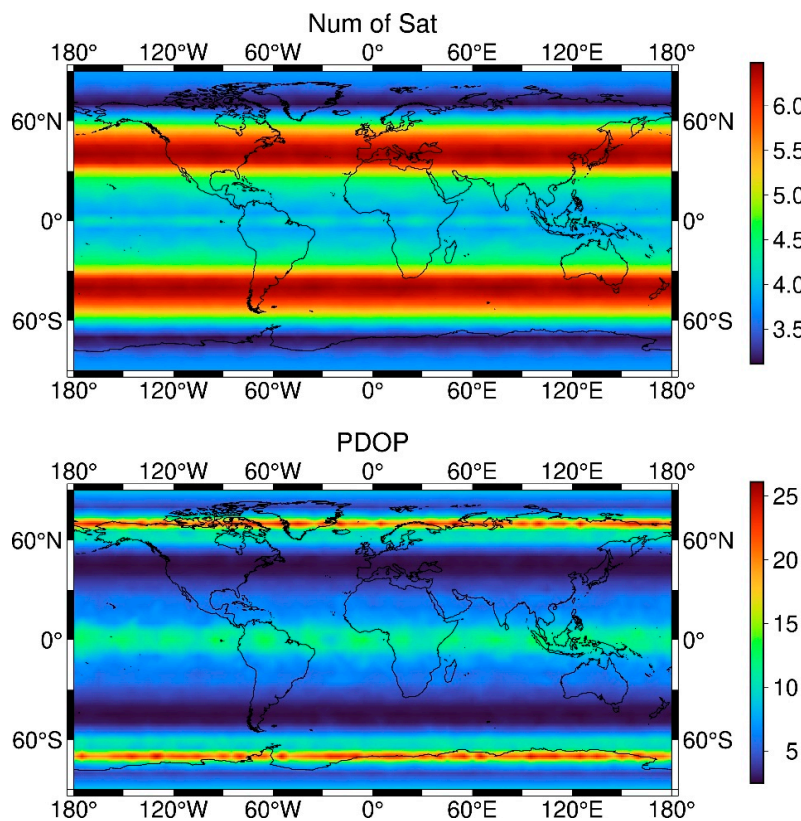


Figure 2. Global distribution for average number of visible satellites (at the top) and the position dilution of precision (PDOP) (at the bottom) of the designed LEO constellation.

2.2. Observation Simulation

Because the simulated LEO satellite was used as the navigation satellite, it could receive observations from GNSS satellites using onboard receiver and transmit navigation signals to ground receivers. However, we focused on the LEO and GNSS observations received from ground tracking stations. Therefore, only the ground observations for LEO, GPS, and BDS-3 satellites were simulated simultaneously. The ground coverage of the LEO satellite was only approximately one-tenth of the MEO satellite because of the lower orbit altitude of the formed [23]. To achieve global GNSS tracking, dozens or even more than 100 ground stations are needed. According to the coverage ratio of 10 to 1 for LEO and GNSS, at least a few hundred ground stations are needed to achieve global tracking of LEO satellites, which is excessively large and difficult to realize. Hence, we only simulated the observation data of 15 regional ground tracking stations to research the estimation strategy of the LEO satellite clock using ground stations. Figure 3 displays the distribution of 15 ground tracking stations used in this study. The red dots denote the ground stations for LEO satellite clock estimation and the blue dots denote the ground stations for LEO-augmented GNSS PPP.

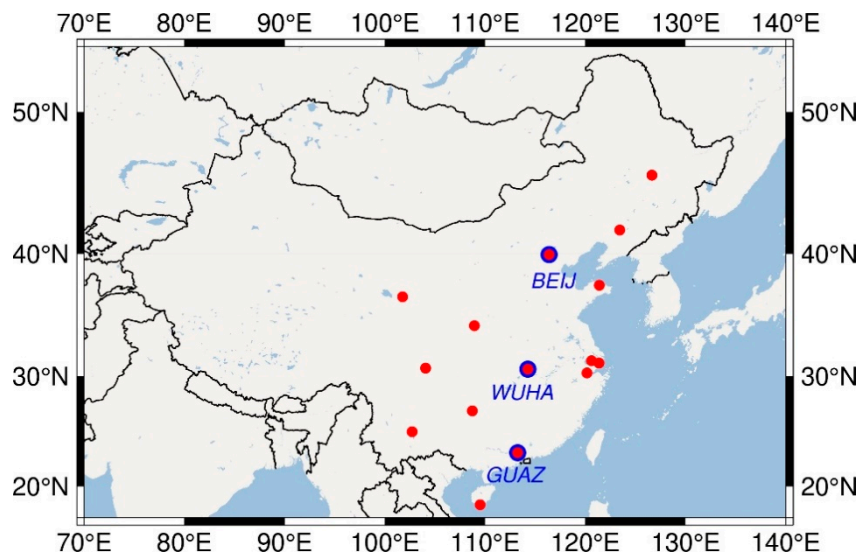


Figure 3. Distribution of regional ground tracking stations. The red dots denote the ground stations for LEO satellite clock estimation, and the blue dots denote the ground stations for LEO-augmented Global Navigation Satellite System (GNSS) precise point positioning (PPP).

The observations received by ground stations from GPS, BDS, and LEO satellites were simulated on the basis of undifferenced code and phase observation equations, which can be expressed as follows:

$$P_{r,j}^s = \rho_{r,j}^s + t_r - t^s + T_r^s + I_{r,j}^s + b_{r,j} - b_j^s + \varepsilon_{r,j}^{s,p} \quad (1)$$

$$L_{r,j}^s = \rho_{r,j}^s + t_r - t^s + T_r^s - I_{r,j}^s + \lambda_j N_{r,j}^s + B_{r,j} - B_j^s + \varepsilon_{r,j}^{s,l} \quad (2)$$

where the super- and subscripts s , r , and j refer to the satellite, receiver, and carrier frequency, respectively; $P_{r,j}^s$ and $L_{r,j}^s$ are undifferenced code and phase observations, respectively; $\rho_{r,j}^s$ denotes the geometric distance between the phase center of the satellite and the receiver antenna; t^s and t_r are the clock offsets of the satellite and receiver, respectively; λ is the carrier wavelength; $N_{r,j}^s$ is the phase ambiguity; $b_{r,j}$ and b_j^s refer to the code hardware delays of receiver and satellite; $B_{r,j}$ and B_j^s are the phase delays of receiver and satellite, respectively; $I_{r,j}^s$ and T_r^s refer to the slant ionospheric and tropospheric delays, respectively; $\varepsilon_{r,j}^{s,p}$ and $\varepsilon_{r,j}^{s,l}$ are the observations' noise of the code and phase. The dual-frequency observation data of GPS, BDS-3, and LEO were simulated and processed.

The main objective of observation simulation was to calculate the sum of the right-hand terms of the simulated code and phase observation Equations (1) and (2). The $\rho = \sqrt{(X^s - X_r)^2 + (Y^s - Y_r)^2 + (Z^s - Z_r)^2}$ is the geometric distance between a receiver of the ground station and a satellite observed by this receiver, which is the main calculated value of the simulation. The (X^s, Y^s, Z^s) and (X_r, Y_r, Z_r) represent the station and receiver coordinates, respectively. The phase center offset (PCO) and phase center variation (PCV) corrections were considered in the process of calculating these geometric distances. The satellite positions were obtained from the STK software. The antenna phase center model igs08.atx from the International GNSS Services (IGS) [28] was applied to existing GPS and BDS satellites, whereas these corrections of new BDS-3 and LEO satellites were set to zero. The satellite clock for existing GPS and BDS satellites was obtained from precise clock products, while the old satellites clocks were used for the new BDS-3 and LEO satellites. The receiver clock was obtained in accordance with the same receiver type of precise clock products. The slant tropospheric delay was represented using zenith tropospheric delay and the mapping function. The Saastamoinen model [29] and global mapping function (GMF) [30] were applied to the slant tropospheric delay. Since the ionosphere-free (IF) linear combinations were used in this study, the ionospheric delay was not considered in the simulation observation equations to simplify the simulation process. The ambiguity was simulated by setting an integer constant for each continuous arc. The code bias was assumed on the basis of the multi-GNSS differential code bias products. The observation noise was simulated as white noise, whose standard deviations (STDs) were 1 m and 5 mm for code and phase observations in the zenith direction, respectively. As the altitude angle declined, additional noise was added appropriately to ensure the vraisemblance of the simulated data. The satellite elevation mask angle of receivers was set as 1° in the simulation.

3. Methods

After the constellation and observation data of LEO, GPS, and BDS-3 were simulated, the method of the LEO satellite clock estimation and LEO-augmented GNSS PPP with the estimated LEO satellite clock were introduced in this section.

3.1. LEO Satellite Clock Estimation

In the process of estimating the LEO satellite clock, the IF linear combinations of code and carrier phase observations were used to eliminate the ionospheric delay [2]. The IF combination of Equations (1) and (2) can be written as

$$P_{r,IF}^s = \rho_{r,IF}^s + \bar{t}_r - \bar{t}^s + T_r^s + \varepsilon_{r,IF}^{s,p} \quad (3)$$

$$L_{r,IF}^s = \rho_{r,IF}^s + \bar{t}_r - \bar{t}^s + \lambda_{IF} \bar{N}_{r,IF}^s + T_r^s + \varepsilon_{r,IF}^{s,l} \quad (4)$$

with

$$\begin{cases} \bar{t}_r = t_r + b_{r,IF} \\ \bar{t}^s = t^s + b_{IF}^s \\ \bar{N}_{r,IF}^s = N_{r,IF}^s + (B_{r,IF} - B_{IF}^s - b_{r,IF} + b_{IF}^s) / \lambda_{IF} \end{cases} \quad (5)$$

where \bar{t}_r and \bar{t}^s refer to the estimable receiver and satellite clock, which absorb the IF code hardware delays of the receiver and satellite, respectively [31]; λ_{IF} is the carrier wavelength for IF combination; $B_{r,IF}$, B_{IF}^s , $b_{r,IF}$, and b_{IF}^s are IF code and phase biases for satellite and receiver, respectively; $N_{r,IF}^s$ is the original ambiguity for IF combination; and $\bar{N}_{r,IF}^s$ is the estimable ambiguity for IF combination, which absorbs the code and phase hardware delays of satellite and receiver.

Although we paid no attention to the onboard GNSS observations from LEO satellites in this study, the LEO onboard observations were also related to the LEO clock as LEO observations from the

ground receivers. The LEO onboard GNSS observation and ground LEO observation can be expressed as follows:

$$P_{L,IF}^s = \rho_{L,IF}^s + \bar{t}_L - \bar{t}^s + \varepsilon_{L,IF}^{s,p} \quad (6)$$

$$P_{r,IF}^L = \rho_{r,IF}^L + \bar{t}_r - \bar{t}^L + T_r^L + \varepsilon_{r,IF}^{L,p} \quad (7)$$

where L represents the LEO satellite when it is in the superscript and the LEO onboard receiver when it is in the subscript; and \bar{t}^L and \bar{t}_L stand for the estimable LEO onboard receiver clock and LEO satellite clock, respectively. Li et al. [22] imposed an equal constraint on the two clocks to increase the contribution of LEO ground observations. However, they are unequal due to the absorption of different code delays during receiving and transmitting signals. The difference between the two clocks can be derived as follows:

$$\bar{t}^L - \bar{t}_L = (t^L - t_L) - (b_{IF}^L - b_{L,IF}) \quad (8)$$

with

$$\begin{cases} t^L = t_L \\ b_{IF}^L \neq b_{L,IF} \\ \bar{t}^L \neq \bar{t}_L \end{cases} \quad (9)$$

We assumed that the same synchronized clock was shared when receiving and transmitting navigation signals on the LEO satellite. The difference between the code delays from the LEO onboard receiver and satellite determines the difference between the two clocks. Consequently, we needed to estimate the LEO satellite clock using ground stations.

In the model of LEO satellite clock estimation, we fixed satellite orbits and the coordinates of the ground tracking station. Moreover, the GPS satellite clock was estimated for the comparative analysis of the LEO satellite clock. The inter-system bias (ISB) introduced by the differences between IF code biases from GPS and LEO should be considered. Due to the stable characteristics of ISB parameters, the number of receiver clock parameters for multi-GNSS can be reduced after the introduction of ISB. Thus, the models of GPS and LEO satellite clock estimation can be expressed in accordance with Equations (3) and (4) as

$$p_{r,IF}^G = \bar{t}_{r,G} - \bar{t}^G + m_r z_r + \varepsilon_{r,IF}^{G,p} \quad (10)$$

$$p_{r,IF}^L = \bar{t}_{r,G} - \bar{t}^L + ISB_r^{GL} + m_r z_r + \varepsilon_{r,IF}^{L,p} \quad (11)$$

$$l_{r,IF}^G = \bar{t}_{r,G} - \bar{t}^L + \lambda_{IF} \bar{N}_{r,IF}^G + m_r z_r + \varepsilon_{r,IF}^{G,l} \quad (12)$$

$$l_{r,IF}^L = \bar{t}_{r,G} - \bar{t}^L + ISB_r^{GL} + \lambda_{IF} \bar{N}_{r,IF}^L + m_r z_r + \varepsilon_{r,IF}^{L,l} \quad (13)$$

with

$$\begin{cases} \bar{t}_{r,G} = t_r + b_{r,IF}^G \\ ISB_r^{GL} = b_{r,IF}^L - b_{r,IF}^G \end{cases} \quad (14)$$

where $p_{r,IF}^G$, $p_{r,IF}^L$, $l_{r,IF}^G$, and $l_{r,IF}^L$ denote the observed-minus-computed code and phase observations of GPS and LEO, which eliminate geometrical distance and troposphere dry delay, and so on; ISB_r^{GL} represents the ISB parameters between GPS and LEO; z_r is the zenith wet troposphere delay parameter; and m_r is the mapping function.

The clock parameters of both receiver and satellite and ISB parameters were estimated simultaneously. Hence, two zero-mean conditions should be introduced to make these parameters uniquely solvable [22]. One condition was introduced for all satellite clocks to remove the linear dependence among receiver and satellite clocks, as indicated in Equation (15). The other condition was introduced for all estimated ISBs to remove the linear dependence between the satellite clock and ISBs, as presented in Equation (16).

$$\sum \bar{t}^s = 0 \quad (15)$$

$$\sum ISB_r = 0 \quad (16)$$

3.2. LEO-Augmented GNSS PPP

To further analyze the precision of the LEO satellite clock estimated using ground tracking stations, we assessed the performance of LEO-augmented GNSS PPP with the estimated LEO satellite clock. In the process of LEO-augmented GNSS PPP, the observations from all GPS, BDS, and LEO satellites were processed, and all satellite orbits and clocks were fixed. IF observations were also used to eliminate the ionosphere effect, and the models of LEO-augmented GNSS PPP were provided as

$$p_{r,IF}^G = -u_r^G r + \bar{t}_{r,G} + m_r z_r + \varepsilon_{r,IF}^{G,p} \quad (17)$$

$$p_{r,IF}^C = -u_r^C r + \bar{t}_{r,G} + ISB_r^{GC} + m_r z_r + \varepsilon_{r,IF}^{C,p} \quad (18)$$

$$p_{r,IF}^L = -u_r^L r + \bar{t}_{r,G} + ISB_r^{GL} + m_r z_r + \varepsilon_{r,IF}^{L,p} \quad (19)$$

$$l_{r,IF}^G = -u_r^G r + \bar{t}_{r,G} + \lambda_{IF} \bar{N}_{r,IF}^G + m_r z_r + \varepsilon_{r,IF}^{G,l} \quad (20)$$

$$l_{r,IF}^C = -u_r^C r + \bar{t}_{r,G} + ISB_r^{GC} + \lambda_{IF} \bar{N}_{r,IF}^C + m_r z_r + \varepsilon_{r,IF}^{C,l} \quad (21)$$

$$l_{r,IF}^L = -u_r^L r + \bar{t}_{r,G} + ISB_r^{GL} + \lambda_{IF} \bar{N}_{r,IF}^L + m_r z_r + \varepsilon_{r,IF}^{L,l} \quad (22)$$

where u_r^s refers to the line-of-sight vector from the receiver antenna to the satellite; r is the vector of receiver antenna position corrections relative to the initial position; and $ISB_r^{GC} = b_{r,IF}^C - b_{r,IF}^G$ denotes the ISB parameters between GPS and BDS. The rest of formulas have identical implication with those in the above.

3.3. Data Processing Strategy

A weekly set of observations for the 15 stations shown in Figure 3 from DOY 305 to 311, 2019, were processed to assess the performance of precise clock estimation (PCE) for the LEO satellite and LEO-augmented GNSS PPP, which were simulated following the simulation strategy presented in Section 2. The data processing strategy and observation models for PCE and LEO-augmented GNSS PPP are summarized in Table 2. In the process of LEO PCE, the GPS satellite clocks were estimated to compare and analyze the convergence time and precision of the LEO satellite clocks. LEO precise satellite clock products with 5-s intervals were estimated using undifferenced code and phase observations. In the process of GNSS PPP, the observations from all LEO, GPS, and BDS satellites were processed to analyze and compare the augmented effects of LEO and BDS with 1-s sampling interval. Moreover, the satellite and receiver antenna phase center was corrected with a similar strategy to that used for the simulated data. The tropospheric dry delay can be precisely corrected using the priori model. Hence, we only estimated the zenith wet troposphere delay with a random walk process. The prior observation noise was set to 5 mm for phase and 1.0 m for code, and the elevation-dependent weight was used. We read the observation data from the Receiver Independent Exchange (RINEX) file to simulate the real-time estimation mode.

Table 2. Data processing strategy and observation models for LEO precise clock estimation (PCE) and LEO-augmented GNSS PPP.

Items	Description
Satellites	168 LEO + 24 GPS + 30 BDS
Estimator	LSQ in sequential mode
Observations	Undifferenced code and phase observations
Signal selection	GPS: L1/L2; BDS: B1C/B2a; LEO: L1/L2
Elevation mask	7°
Sampling interval	5 s for PCE and 1 s for PPP
Weighting	Priori precision 5 mm for phase and 1.0 m for code; Elevation-dependent weight
Relativistic effect	IERS Conventions 2010
Tropospheric delay	Initial model (Saastamoinen [29] and GMF [30]) and random-walk process
Ionospheric delay	IF combination
Station displacement	Solid Earth tide, pole tide, ocean loading tide
Satellite antenna phase center	PCO and PCV corrected for GPS and BDS using igs08.atx [28]; none for LEO
Receiver antenna phase center	PCO and PCV corrected for GPS and only PCO corrected for BDS using igs08.atx [28]; none for LEO
Phase wind-up	Corrected
ISB	Estimated as constant
Station coordinate	Fixed for PCE; Estimated in static mode for PPP
Satellite orbit	Fixed with the simulated precise orbit products from STK software
Satellite clocks	Estimated with white noise for PCE; Fixed with the products from PCE for LEO PPP; Fixed with the simulated precise clock products for GPS and BDS PPP
Receiver clocks	Estimated with white noise
Ambiguities	Constant for each arc

4. Analysis of Results

In this section, the results of the LEO satellite clock estimated using the methods in Section 3.1 are assessed and compared with the results of the GPS satellite clock, including convergence speed and precision. Then, we analyze the convergence speed of the LEO and GPS satellite clock from the perspective of satellite TDOP, which is calculated by one satellite relative to multiple ground tracking stations. Lastly, the performance of LEO-augmented GNSS PPP solutions with the real-time estimated LEO satellite clock are analyzed to assess the quality of the estimated LEO satellite clock.

4.1. Analysis of LEO Satellite Clock

To assess the results of the LEO satellite clock, we computed the differences between the simulated and estimated precise clocks. The resulting clock time series were aligned to a reference satellite to remove systematic biases using the standard clock comparisons practice [32]. We used the average of the GPS satellite clock differences as a relatively stable reference satellite instead of a fixed satellite due to the short arc length of the LEO satellite and the adoption of regional tracking stations.

Figure 4 shows the convergence series of the segmental LEO satellite clock compared with GPS satellite within 6 h for DOY 305, 2019, after the removal of satellite-specific mean biases. L in front of the pseudo random noise (PRN) number indicates the LEO satellite. It can be clearly observed that GPS satellites were tracked continuously for several hours, whereas most of LEO satellites were interrupted for approximately 20 min in Figure 4. The solution of GPS satellite clock was regarded as being converged when the clock difference remained less than the threshold of 0.2 ns for more than 5 min in this study. It was obviously not suitable to use the convergence threshold of the GPS satellite for LEO satellite. Therefore, we used the triple-mean square error of LEO satellite clocks for the last 3 min tracked using ground stations as the threshold of convergence. Because the averaged triple-mean square error for LEO satellite clocks is 0.79 ns, the threshold of convergence was set as 0.8 ns and the continuous-time was set as 1 min for LEO. The convergence time of the GPS satellite clock was approximately 30 min, whereas the time of the LEO satellite clock was only within 3 min in Figure 4. The faster convergence of the LEO satellite clock resulted from the lower orbital altitudes and faster motion of LEO satellites compared with those of GPS satellites.

We estimated the LEO satellite clock from DOY 305 to 311, 2019, for all simulated LEO and GPS satellites to analyze the estimated LEO satellite clock comprehensively. Differenced with the simulated

precise clock products, Figure 5 demonstrates the statistical results about convergence time, RMS, and STD after convergence averaged over DOY 305–311, 2019, for LEO and GPS satellites. The three subplots on the left represent LEO satellites and the three subplots on the right represent GPS satellites for comparison. Table 3 illustrates the average convergence time, RMS, and STD for all LEO and GPS satellite clocks based on Figure 5. The convergence time of LEO satellite clock was considerably lower than that of the GPS satellite clock, which is consistent with the results shown in Figure 3. The average convergence time was 2.86 min for the LEO satellite clock, whereas the value was 31.21 min for the GPS satellite clock. The average RMS and STD values after convergence were 0.71 ns and 0.39 ns for LEO satellite clock, respectively, whereas the values were 0.31 ns and 0.13 ns for the GPS satellite clock. The RMS and STD after convergence of the LEO satellite clock were slightly higher than those of the GPS satellite clock in Figure 5 and Table 3. Such a difference was caused by the exact short tracking arcs of LEO satellites.

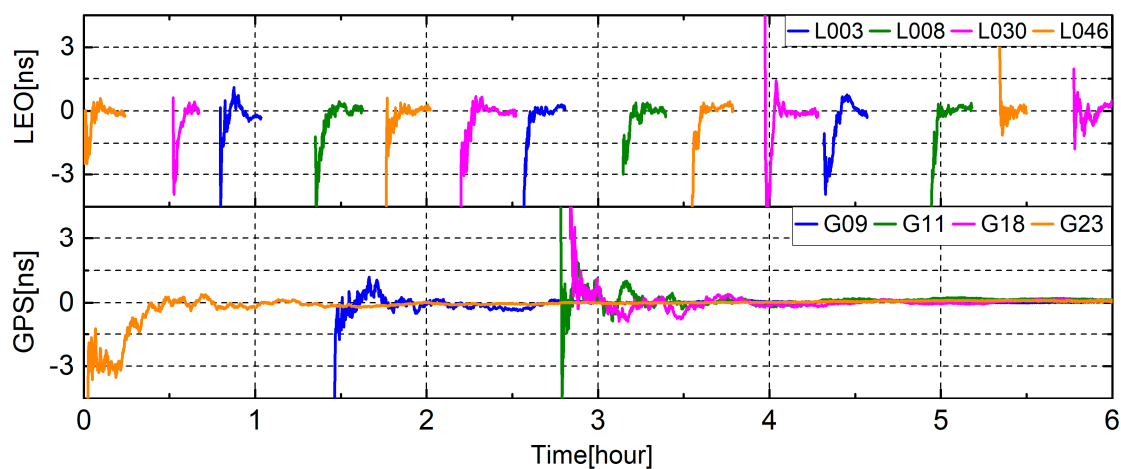


Figure 4. Convergence series of segmental LEO and GPS satellite clock within 6 h for the day of year (DOY) 305, 2019. The top picture denotes four LEO satellites (L003, L008, L030, and L046) and the bottom picture denotes four GPS satellites (G09, G11, G18, and G23).

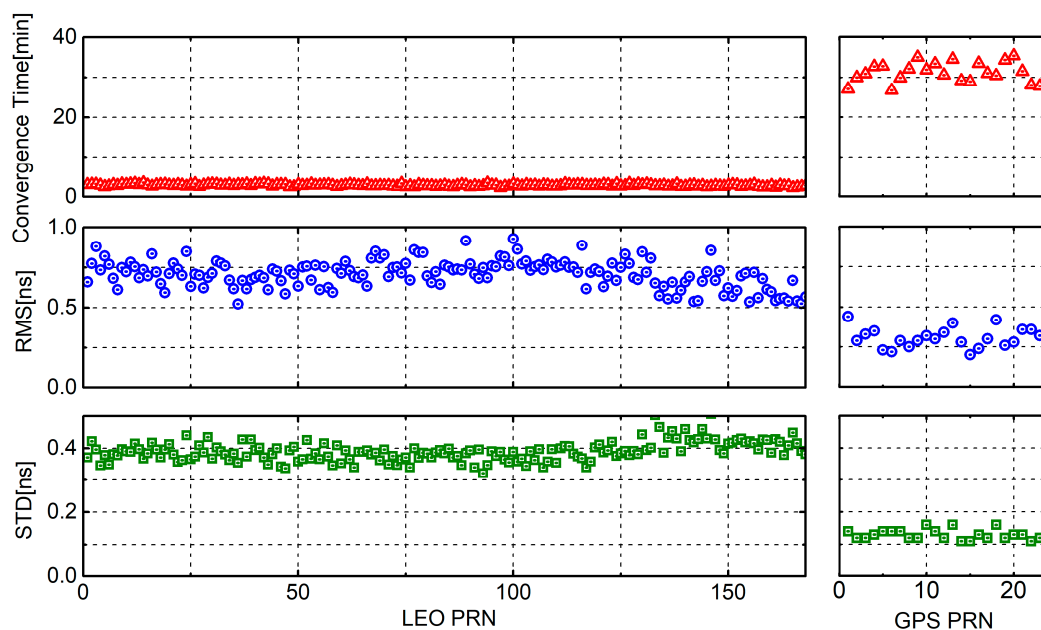


Figure 5. Convergence time, root mean square (RMS), and STD of the estimated satellite clock averaged over DOY 305–311, 2019, for LEO (the three subplots on the left) and GPS (the three subplots on the right) satellites compared with the simulated precise clock.

Table 3. Average convergence time, RMS, and STD after convergence for 168 LEO and 24 GPS satellite clocks from DOY 305 to 311, 2019.

System	Convergence Times [min]	RMS [ns]	STD [ns]
LEO	2.86	0.71	0.39
GPS	31.21	0.31	0.13

The sky plot for GPS and LEO satellites within 1 h at WUHA station is shown in Figure 6. The red and blue subplots represent LEO and GPS satellites in Figure 6, respectively. We can discover that LEO satellites, including LEO orbit A and B, have the longer arc of motion than the GPS satellites at the same time. This combined constellation allowed more LEO satellites to be observed in the regions of middle latitude. Lower orbital altitudes and faster geometric change of LEO satellites are not only critical for PPP convergence but also for the convergence of the LEO satellite clock.

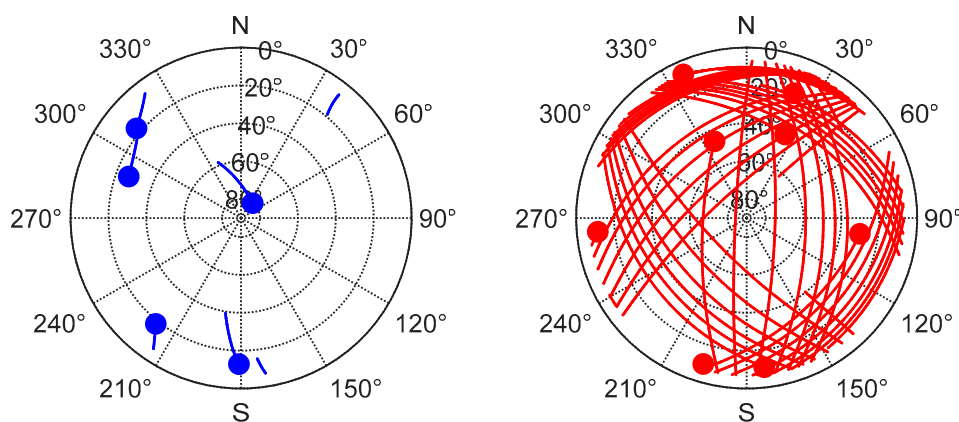


Figure 6. The sky plot for GPS and LEO satellites within 1 h at WUHA station. The red and blue subplots represent LEO and GPS satellites, respectively.

We calculated the number of ground tracking stations where one satellite could be observed, satellite TDOP that one satellite is relative to multiple ground tracking stations, to further analyze the reason for the rapid convergence of the LEO satellite clock. The TDOP factor was related only to the geometric distribution of satellites or stations and could reflect the quality of clock estimation. The delta TDOP caused by satellite motion was also calculated using the difference between the TDOP values of two adjacent epochs. Figure 7 presents the number of visible stations, satellite TDOP, and delta TDOP for LEO and GPS satellites observed using tracking stations within an hour for DOY 305, 2019. It was found that the number of visible stations where one satellite can be observed changed remarkably for LEO, whereas the number of visible stations for the GPS satellite changed slowly. The satellite TDOP for LEO was within 150 and less than 10 when the number of visible stations was large (more than 10). By contrast, the satellite TDOP for GPS was excessively large, such that it reached 300 or more when all ground tracking stations could observe this satellite, and it will even be more than 1000 when the number of visible stations is less than 10. This phenomenon resulted from the different orbit altitude. The orbit altitude of the GPS satellite reached 20,000 km, whereas that of LEO was lower than 1000 km. The values of delta TDOP for LEO and GPS satellites were relatively close, and both were less than 1.

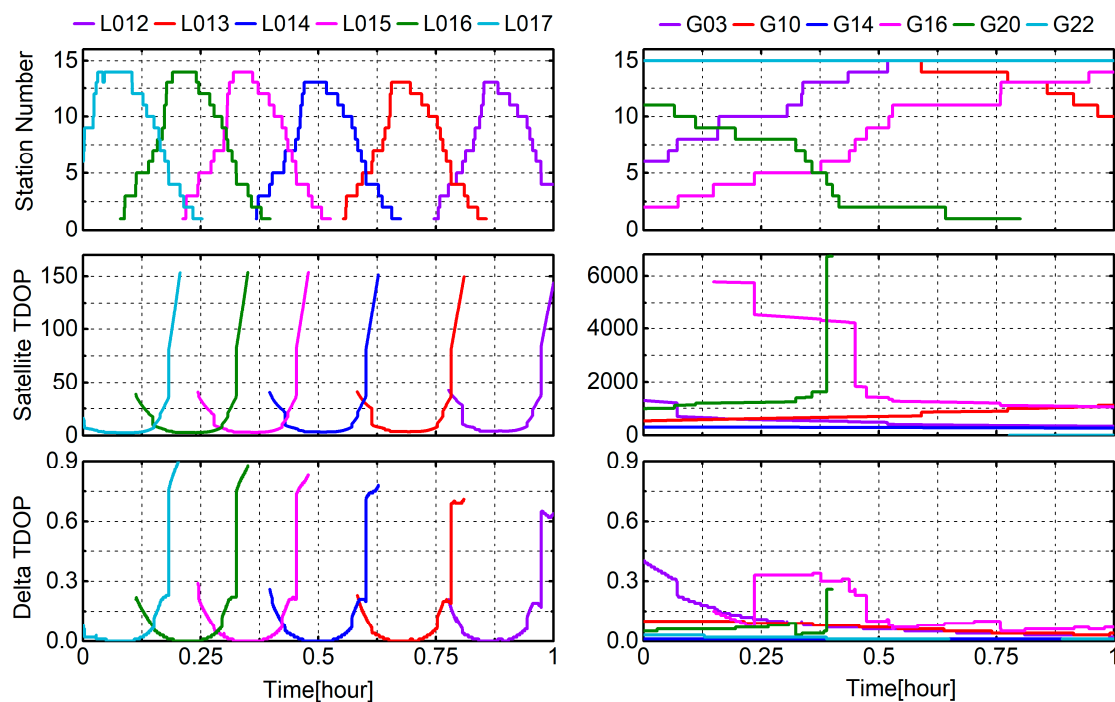


Figure 7. Number of visible stations where one satellite can be observed, satellite time dilution of precision (TDOP), and delta TDOP for LEO and GPS satellites for 1 h. The satellite TDOP was calculated using one satellite relative to multiple ground tracking stations.

We estimated the number of visible stations, satellite TDOP, and delta TDOP from DOY 305 to 311, 2019, for all simulated LEO and GPS satellites to analyze the convergence speed of the LEO satellite clock comprehensively. Figure 8 presents the number of visible stations, satellite TDOP, and delta TDOP averaged over DOY 305–311, 2019, for LEO and GPS satellites. Table 4 expresses the average number of visible stations, satellite TDOP, and delta TDOP for 168 LEO satellites and 24 GPS satellites from DOY 305 to 311, 2019. Figure 8 and Table 4 indicate that the number of stations observed by the LEO satellite was slightly lower than that of the GPS satellite. The average number of visible stations for 168 LEO satellites and 24 GPS satellites were 7.19 and 11.46, respectively. This condition was caused by the satellite footprint, and the footprint diameter of LEO satellite was approximately 3000 km in this study, whereas that of GPS satellite was approximately 12,000 km [33]. Similar to the results in Figure 7, the satellite TDOP averaged weekly for the LEO satellite was much smaller than that for the GPS satellite. The average satellite TDOPs for 168 LEO satellites and 24 GPS satellites were 19.13 and 1294.70, respectively. The average delta TDOPs for 168 LEO satellites and 24 GPS satellites were both 0.10. Nevertheless, in Figure 8, with an increase in satellite PRN, the three values, namely, number of visible stations, satellite TDOP, and delta TDOP, for LEO satellite were more concentrated, whereas those values for GPS satellites were relatively scattered, especially satellite TDOP and delta TDOP. This phenomenon resulted from the different orbits' periods of the satellite.

Table 4. Average number of visible stations, satellite TDOP, and delta TDOP for 168 LEO satellites and 24 GPS satellites from DOY 305 to 311, 2019.

System	Station Numbers	Satellite TDOP	Delta TDOP
LEO	7.19	19.13	0.10
GPS	11.46	1294.70	0.10

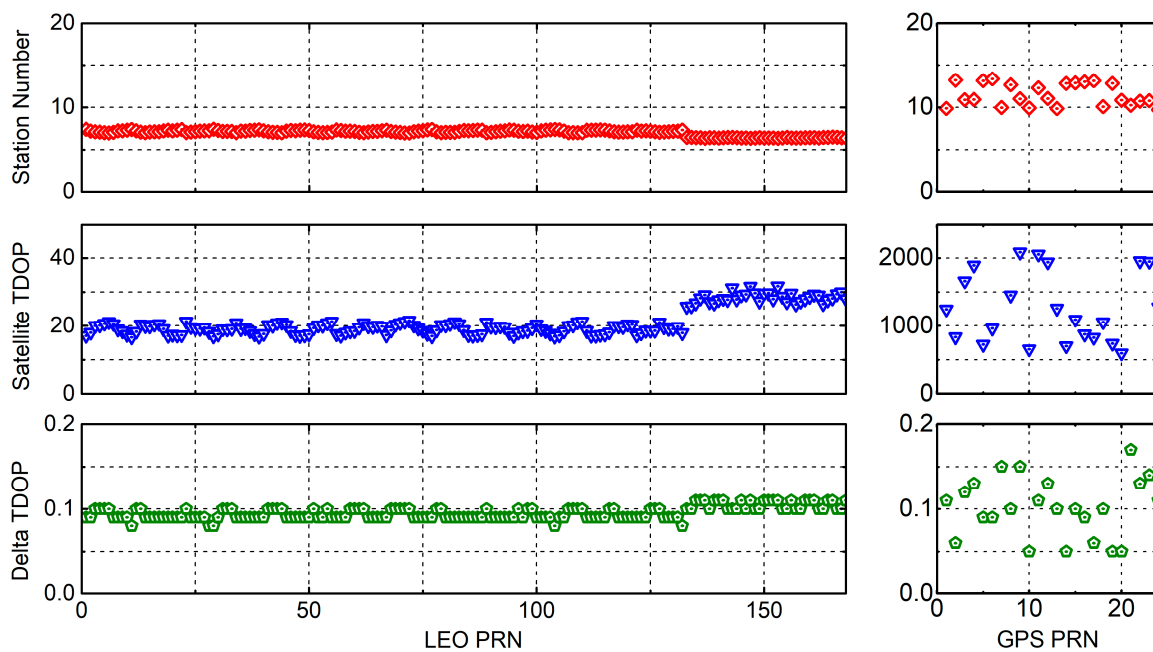


Figure 8. Number of visible stations, satellite TDOP, and delta TDOP averaged over DOY 305–311, 2019, for LEO and GPS satellites.

4.2. Analysis of LEO-Augmented GNSS PPP

The performance of LEO-augmented GNSS PPP solutions with real-time estimated LEO satellite clock was analyzed and compared with the simulated precise clock to evaluate the quality of the estimated LEO satellite clock further. Figure 3 shows the locations of three stations for analyzing the PPP performance, named BEIJ, WUHA, and GUZH. The PPP solution was regarded as being converged when the positioning errors were less than 10 cm and 20 cm in horizontal and vertical directions, respectively, for more than 20 epochs.

Figure 9 presents comparisons of GPS-only, GPS/BDS, and GPS/LEO PPP solutions with the estimated LEO satellite clock at stations BEIJ, WUHA, and GUZH for DOY 305, 2019. It was found that the participation of LEO satellites did not improve the number of visible satellites and PDOP as remarkably as BDS satellites did. The average number of visible satellites and PDOP values for GPS/BDS were 19.58 and 1.18, respectively, whereas that values for GPS/LEO were 12.43 and 1.34, respectively. However, LEO could still accelerate PPP convergence more substantially than BDS with the real-time estimated LEO satellite clock. The average convergence time for GPS/BDS and GPS/LEO PPP was 26.12 min and 10.87 min, respectively. Although additional errors of the LEO satellite clock were introduced into the positioning results, the rapid variation in PDOP values caused by the rapid movement of LEO satellites was sufficient to compensate for this shortcoming.

Figure 10 shows comparisons of LEO-augmented GNSS PPP solutions for GPS/BDS/LEO (with the estimated LEO satellite clock) and GPS/BDS/LEO0 (with the simulated precise clock) at station WUHA for DOY 305, 2019. The subscript 0 means the use of the simulated precise clock as a reference. As we can see, the convergence time of LEO-augmented GNSS PPP with the estimated LEO satellite clock was slightly longer than that with the simulated precise clock. This result was not only caused by errors in the real-time estimated LEO satellite clock, but a few minutes of the convergence time of the LEO satellite clock also exacerbated this effect. Nonetheless, the participation of LEO satellites can still substantially shorten the convergence time of GNSS PPP with the real-time estimated LEO satellite clock.

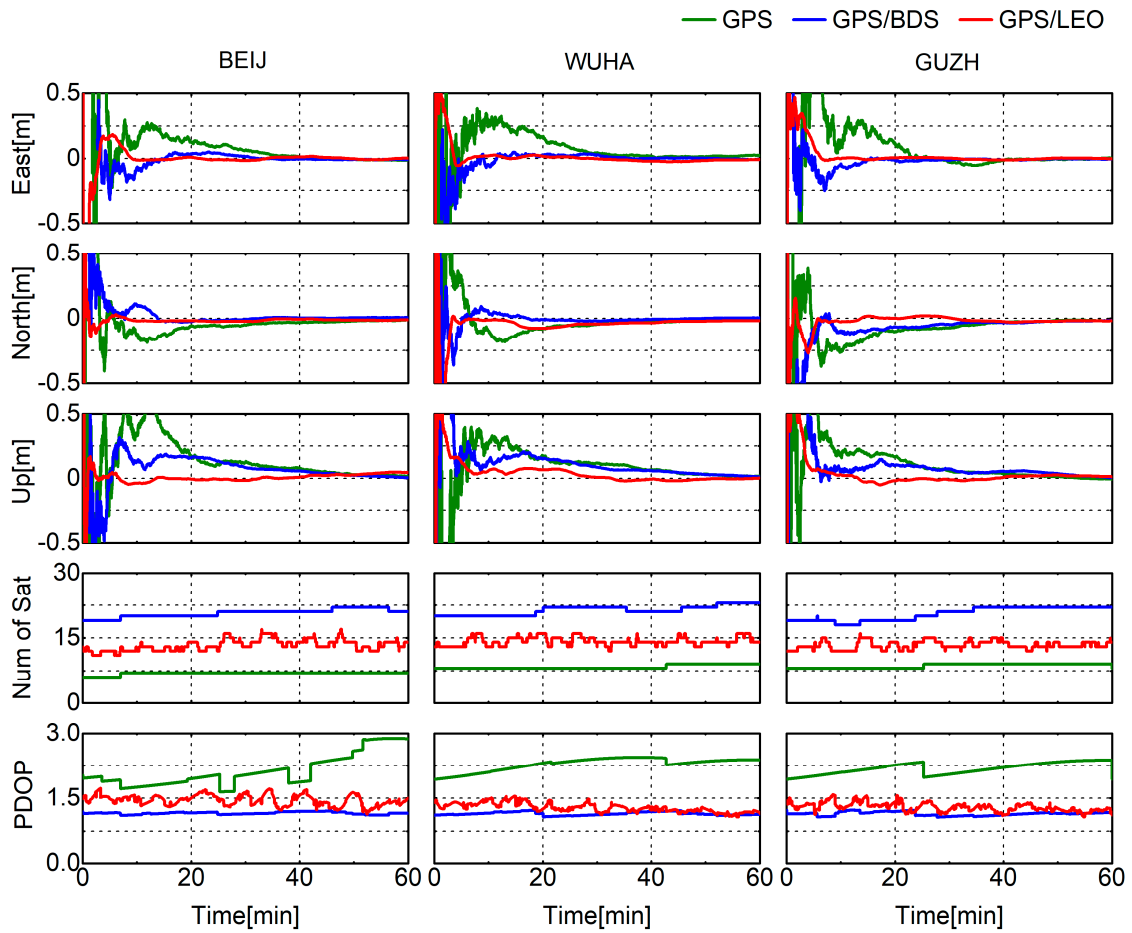


Figure 9. Comparisons of GPS-only, GPS/BDS, and GPS/LEO PPP solutions in east, north, and up directions, number of visible satellites, and PDOP, with estimates of LEO satellite clock at stations BEIJ, WUHA, and GUZH.

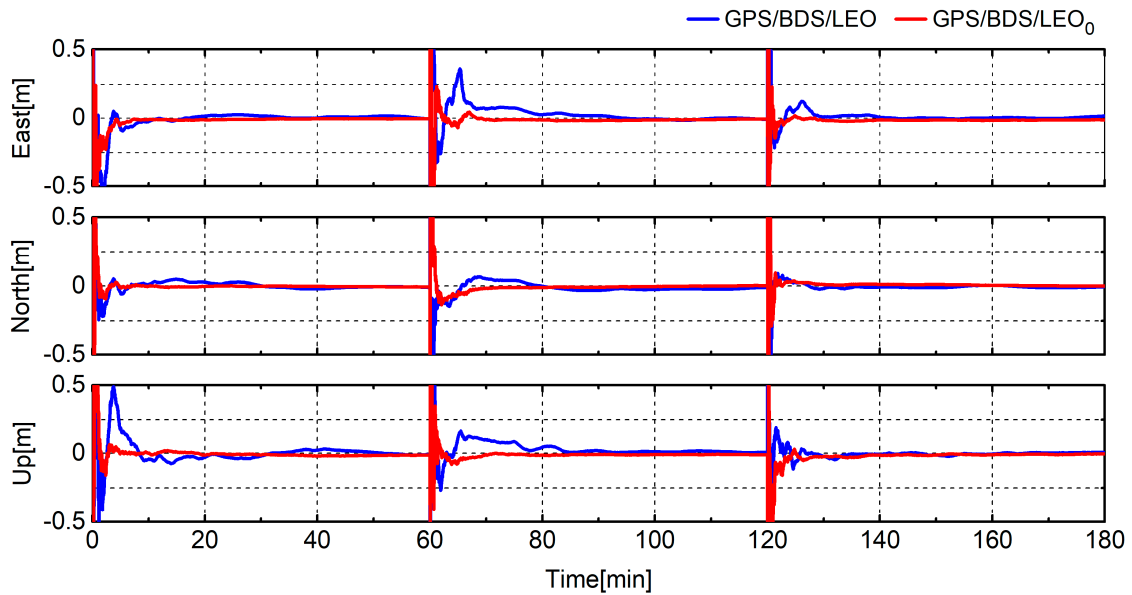


Figure 10. LEO-augmented GNSS PPP solutions for GPS/BDS/LEO (with the estimated LEO satellite clock) and GPS/BDS/LEO₀ (with the simulated precise clock) at station WUHA for DOY 305, 2019.

We computed PPP solutions from DOY 305 to 311, 2019, for GPS-only, GPS/BDS, GPS/LEO, GPS/BDS/LEO, and GPS/BDS/LEO₀ at stations BEIJ, WUHA, and GUZH to analyze the performance of LEO-augmented GNSS PPP solutions with the real-time estimated LEO satellite clock comprehensively. The processes of PPP calculation were restarted every 2 h to acquire more information about convergence time. Figure 11 shows the statistical results about the convergence time, number of satellite, PDOP value, and positioning errors in east, north, and up components after convergence averaged for 7 days. It can be obviously found that the augmented effect of LEO on GPS PPP was better than that of BDS with the estimated LEO satellite clock, especially in convergence time. The former shortened the convergence time and improve the positioning accuracy by 66%, 43%, 34%, and 35% in the east, north, and up components, respectively, which is consistent with the results in Figure 9. The convergence time and positioning accuracy for LEO-augmented GNSS with the estimated LEO satellite clock reached 10.63 min, 1.94 cm, 1.44 cm, and 4.18 cm in the east, north, and up components, respectively. The improvements caused by LEO satellite for GPS/BDS PPP were 59%, 30%, 31%, and 33%, respectively.

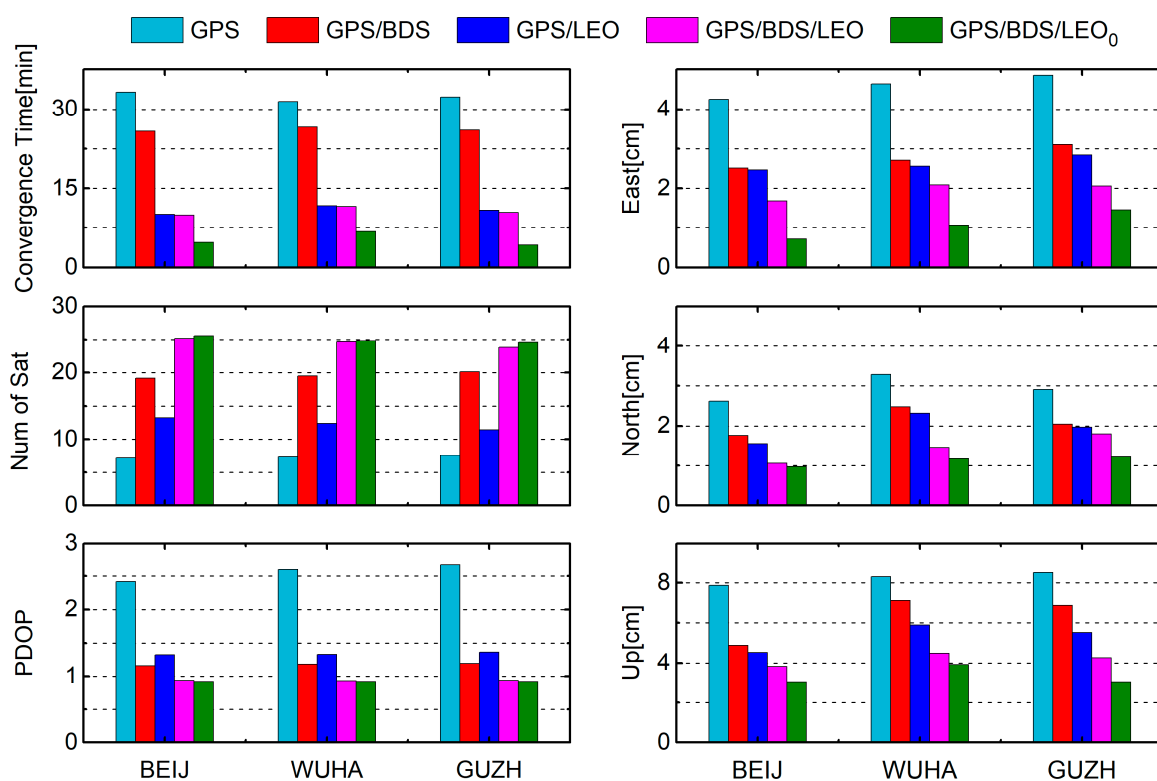


Figure 11. Convergence time, number of satellite, PDOP value, and positioning errors in east, north and up components after convergence of GPS-only, GPS/BDS, GPS/LEO, GPS/BDS/LEO, and GPS/BDS/LEO₀ averaged over DOY 305–311, 2019, at stations BEIJ, WUHA, and GUZH.

Although the augmented effect of LEO satellites on GNSS PPP with the estimated LEO satellite clock was substantial, it was still slightly behind that with the simulated precise clock. Due to the existence of convergence times and errors of the estimated LEO satellite clock, the convergence times and positioning errors of GPS/BDS/LEO PPP with the estimated LEO satellite clock could not reach the level of using the simulated LEO satellite lock. Our future work is to improve the accuracy of the estimated LEO satellite clock, thereby shortening the difference with the simulated LEO satellite clock. When the characteristic of the difference between the LEO receiver and satellite clock is clear, the accuracy and continuity of the LEO satellite clock are expected to be close to the simulated precise clock with the participation of LEO onboard observations.

5. Discussion

The estimation approach of this study is preliminary research for the issue of LEO satellite clock, although the augmented effect of LEO satellites with the estimated LEO satellite clock using ground stations is substantial. The next research on the LEO clock problem requires the participation of onboard observations to provide continuous LEO clock service. The rapid convergence of the LEO satellite clock made it possible to determine the characteristics of the difference between the two clocks when the continuous LEO onboard receiver clock was estimated using the LEO onboard observations. Only by calibrating the LEO onboard receiver clock with the estimated satellite clock based on ground stations or by joint estimation of LEO receiver and satellite clocks based on the observation from the ground and LEO onboard receivers can the issue of the LEO satellite clock be solved.

The distribution of the ground tracking stations' network is significant. For global LEO satellite clock estimation, the ground tracking stations should be distributed as evenly as possible. For regional LEO satellite clock estimation, the LEO satellites need to be monitored continuously as long as possible. For LEO-augmented GNSS PPP, the rover station needs to be within the service range of the ground tracking stations providing LEO satellite clock products. In order to obtain a reliable network of ground tracking stations, the time of tracking satellites should be as long as possible when the cost of building the station allows. The number of visible stations where one satellite can be observed and the satellite TDOP that one satellite is relative to multiple ground tracking stations are also crucial to the reliability of the tracking network.

With the rapid development of commercial LEO constellations, hundreds and thousands of LEO satellites will bring opportunities for meteorology research. More available satellites and observation periods will dramatically increase the available number of slant wet delays. The rapid movement of LEO satellites makes it possible to obtain more effective observations in a short time, thereby improving the time resolution of atmospheric processes. The longer the arc of the LEO satellite, the greater the change in altitude and azimuth angle, and the greater the effective monitoring range. Real-time estimation of the LEO satellite clock and PPP also provides the possibility of real-time acquisition of tropospheric delay, which will facilitate rapid modeling of the atmosphere. After the ambiguity of the reference station is fixed, more abundant and reliable atmospheric delay information can be extracted due to the participation of LEO satellites. Therefore, adding effective atmospheric constraints can further speed up PPP convergence significantly.

6. Conclusions

This study investigated a real-time estimation approach for the LEO satellite clock based on ground tracking stations. The feasibility for the rapid convergence of the LEO satellite clock was analyzed using the satellite TDOP that one satellite is relative to multiple ground tracking stations. On the basis of the simulated LEO constellation and the observation data from ground tracking stations, the LEO satellite clock for all simulated LEO satellites and LEO-augmented GNSS PPP solutions with the real-time estimated LEO satellite clock for three ground stations from DOY 305 to 311, 2019, were estimated to verify the proposed method.

The convergence time in the estimation process and the accuracy after convergence for the LEO satellite clock were analyzed compared with GPS satellites. Experimental results showed that the LEO satellite clock could be quickly converged in approximately 3 min, and the average RMS and STD values after convergence were 0.71 and 0.39 ns for the LEO satellite clock. The number of ground tracking stations where one satellite could be observed, satellite TDOP and delta TDOP were calculated to further analyze the reason of the rapid convergence for the LEO satellite clock. The average weekly satellite TDOP of the LEO satellite was much smaller than that of the GPS satellite, while the average delta TDOPs caused by satellite motion for all LEO satellites and GPS satellites were the same. Therefore, the rapid convergence of the LEO satellite clock resulted from the better geometric distribution of the LEO satellite relative to ground tracking stations. The short regional tracking time of the LEO satellite resulted in insufficient accuracy and short service time of the real-time LEO satellite

clock. Finally, the performance of LEO-augmented GNSS PPP solutions with the real-time estimated LEO satellite clock was also analyzed to assess the accuracy of the estimated LEO satellite clock. Although the participation of LEO satellites did not improve the number of visible satellites and PDOP as remarkably as BDS satellites did, LEO could still accelerate PPP convergence more substantially than BDS with the estimated LEO satellite clock. The improvements caused by the LEO satellite for GPS/BDS PPP with the real-time estimated LEO satellite clock reached 59%, 30%, 31%, and 33% in the east, north, and up components, respectively. But the augmented effect of LEO satellites on GNSS PPP with the estimated LEO satellite clock was still slightly behind that with the simulated precise clock. It requires joint estimation based on the observation from ground and LEO onboard receivers to further improve the accuracy of the LEO satellite clock.

Author Contributions: Conceptualization, Z.Y. and H.L.; data curation, Z.Y. and L.Z.; formal analysis, Z.Y. and B.S.; methodology, Z.Y., H.L., and C.Q.; writing – original draft preparation, Z.Y. and C.Q.; writing – review and editing, Y.L., X.X., and Y.Z. All authors have read and agreed to the published version of the manuscript.

Funding: This research was funded by the project “Research on Real-time and High-accuracy Multi-GNSS Location Based Service Platform” (No. 2018010401011271), the project “National Key Research and Development Program of China” (No. 2016YFB0800405), and the project “Joint Laboratory of Satellite Navigation Augmentation Theoretical Technology” (No. 250000318).

Conflicts of Interest: The authors declare no conflict of interest

References

1. Zumberge, J.; Heflin, M.; Jefferson, D.; Watkins, M.; Webb, F. Precise point positioning for the efficient and robust analysis of GPS data from large networks. *J. Geophys. Res. Solid Earth* **1997**, *102*, 5005–5017. [[CrossRef](#)]
2. Li, X.; Ge, M.; Dai, X.; Ren, X.; Fritsche, M.; Wickert, J.; Schuh, H. Accuracy and reliability of multi-GNSS real-time precise positioning: GPS, GLONASS, BeiDou, and Galileo. *J. Geod.* **2015**, *89*, 607–635. [[CrossRef](#)]
3. Li, X.; Zhang, X.; Ren, X.; Fritsche, M.; Wickert, J.; Schuh, H. Precise positioning with current multi-constellation global navigation satellite systems: GPS, GLONASS, Galileo and BeiDou. *Sci. Rep.* **2015**, *5*, 8328. [[CrossRef](#)] [[PubMed](#)]
4. Liu, T.; Zhang, B.; Yuan, Y.; Li, M. Real-Time Precise Point Positioning (RTPPP) with raw observations and its application in real-time regional ionospheric VTEC modeling. *J. Geod.* **2018**, *92*, 1267–1283. [[CrossRef](#)]
5. Cai, C.; Gao, Y. Modeling and assessment of combined GPS/GLONASS precise point positioning. *GPS Solut.* **2013**, *17*, 223–236. [[CrossRef](#)]
6. Aggrey, J.; Bisnath, S. Improving GNSS PPP convergence: The case of atmospheric-constrained, multi-GNSS PPP-AR. *Sensors* **2019**, *19*, 587. [[CrossRef](#)] [[PubMed](#)]
7. Cai, C.; Gao, Y.; Pan, L.; Zhu, J. Precise point positioning with quad-constellations: GPS, BeiDou, GLONASS and Galileo. *Adv. Space Res.* **2015**, *56*, 133–143. [[CrossRef](#)]
8. Bisnath, S.; Gao, Y. Current state of precise point positioning and future prospects and limitations. In *Observing Our Changing Earth*; Sideris, M.G., Ed.; Springer: Berlin/Heidelberg, Germany, 2009; Volume 133, pp. 615–623.
9. De Selding, P.B. Signs of a Satellite Internet Gold Rush in Burst of ITU Filings. Available online: <https://spacenews.com/signs-of-satellite-internet-gold-rush/> (accessed on 19 November 2018).
10. Li, D.; Shen, X.; Li, D.; Li, S. On civil-military integrated space-based real-time information service system. *Geomat. Inf. Sci. Wuhan Univ.* **2017**, *42*, 1501–1505.
11. Xiaohong, Z.; Fujian, M. Review of the development of LEO navigation-augmented GNSS. *Acta Geod. Cartogr. Sin.* **2019**, *48*, 1073.
12. De Selding, P.B. SpaceX To Build 4000 Broadband Satellites in Seattle. Available online: <https://spacenews.com/spacex-opening-seattle-plant-to-build-4000-broadband-satellites/> (accessed on 23 October 2018).
13. De Selding, P.B. Virgin, Qualcomm Invest in OneWeb Satellite Internet Venture. Available online: <https://spacenews.com/virgin-qualcomm-invest-in-global-satellite-internet-plan/> (accessed on 28 January 2019).
14. Magan, V. Samsung Exec Envisions LEO Constellation for Satellite Internet Connectivity. Available online: <https://www.satellitetoday.com/telecom/2015/08/18/samsung-exec-envisions-leo-constellation-for-satellite-internet-connectivity/> (accessed on 8 June 2018).

15. De Selding, P.B. Boeing Proposes Big Satellite Constellations in V- and C-bands. Available online: <https://spacenews.com/boeing-proposes-big-satellite-constellations-in-v-and-c-bands/> (accessed on 21 April 2019).
16. De Selding, P.B. Telesat: LEO Gives More User Bandwidth than GEO HTS. Available online: <https://www.spaceintelreport.com/telesat-leo-gives-more-user-bandwidth-than-geo-hts/> (accessed on 15 June 2020).
17. Reid, T.G.; Neish, A.M.; Walter, T.F.; Enge, P.K. Leveraging commercial broadband LEO constellations for navigation. In Proceedings of the ION GNSS 2016, Portland, OR, USA, 12–16 September 2016; pp. 2300–2314.
18. Ke, M.; Lv, J.; Chang, J.; Dai, W.; Tong, K.; Zhu, M. Integrating GPS and LEO to accelerate convergence time of precise point positioning. In Proceedings of the 2015 International Conference on Wireless Communications & Signal Processing (WCSP), Nanjing, China, 15–17 October 2015; pp. 1–5.
19. Li, X.; Ma, F.; Li, X.; Lv, H.; Bian, L.; Jiang, Z.; Zhang, X. LEO constellation-augmented multi-GNSS for rapid PPP convergence. *J. Geod.* **2019**, *93*, 749–764. [[CrossRef](#)]
20. Ge, H.; Li, B.; Ge, M.; Zang, N.; Nie, L.; Shen, Y.; Schuh, H. Initial assessment of precise point positioning with LEO enhanced global navigation satellite systems (LeGNSS). *Remote Sens.* **2018**, *10*, 984. [[CrossRef](#)]
21. Li, X.; Li, X.; Ma, F.; Yuan, Y.; Zhang, K.; Zhou, F.; Zhang, X. Improved PPP ambiguity resolution with the assistance of multiple LEO constellations and signals. *Remote Sens.* **2019**, *11*, 408. [[CrossRef](#)]
22. Li, B.; Ge, H.; Ge, M.; Nie, L.; Shen, Y.; Schuh, H. LEO enhanced Global Navigation Satellite System (LeGNSS) for real-time precise positioning services. *Adv. Space Res.* **2019**, *63*, 73–93. [[CrossRef](#)]
23. Su, M.; Su, X.; Zhao, Q.; Liu, J. BeiDou augmented navigation from low earth orbit satellites. *Sensors* **2019**, *19*, 198. [[CrossRef](#)] [[PubMed](#)]
24. Shen, Y.; Zhang, Y. Design for LEO satellite navigation augmentation system based on integrated communication and navigation. In Proceedings of the 11th China Satellite Navigation Conference (CSNC), Chengdu, China, 23 May 2020; p. 5.
25. Walker, J.G. Satellite constellations. *J. Br. Interplanet. Soc.* **1984**, *37*, 559–572.
26. DOD SPS. *Global Positioning System Standard Positioning Service Performance Standard*, 4th ed.; Department of Defense USA: Washington, DC, USA, 2008.
27. China Satellite Navigation Office (CSNO). *BeiDou Navigation Satellite System Signal in Space Interface Control Document: Open Service Signal, Version 2.1*; China Satellite Navigation Office: Beijing, China, 2016.
28. Schmid, R.; Dach, R.; Collilieux, X.; Jäggi, A.; Schmitz, M.; Dilssner, F. Absolute IGS antenna phase center model igs08. atx: Status and potential improvements. *J. Geod.* **2016**, *90*, 343–364. [[CrossRef](#)]
29. Saastamoinen, J. Atmospheric correction for the troposphere and stratosphere in radio ranging satellites. *Use Artif. Satell. Geod.* **1972**, *15*, 247–251.
30. Böhm, J.; Niell, A.; Tregoning, P.; Schuh, H. Global Mapping Function (GMF): A new empirical mapping function based on numerical weather model data. *Geophys. Res. Lett.* **2006**, *33*. [[CrossRef](#)]
31. Gao, Y. GNSS biases, their effect and calibration. In Proceedings of the IGS Workshop, Miami Beach, FL, USA, 2–6 June 2008.
32. Ge, M.; Douša, J.; Gendt, G.; Wickert, J. A computationally efficient approach for estimating high-rate satellite clock corrections in realtime. *Gps Solut.* **2012**, *16*, 9–17. [[CrossRef](#)]
33. Enge, P.; Ferrell, B.; Bennet, J.; Whelan, D.; Gutt, G.; Lawrence, D. Orbital diversity for satellite navigation. In Proceedings of the ION GNSS 2012, Nashville, TN, USA, 17–21 September 2012; pp. 3834–3845.

